AGU PUBLICATIONS

Geophysical Research Letters

RESEARCH LETTER
10.1002/2017GL073613

Key Points:
- A widespread negative O_2 trend is beginning to emerge from the envelope of interannual variability
- The global ocean O_2 inventory is negatively correlated with the global ocean heat content
- Variability and trends in the observed upper ocean O_2 concentration are dominated by the apparent oxygen utilization

Supporting Information:
- Supporting Information S1
- Figure S1
- Figure S2
- Figure S3
- Figure S4

Correspondence to:
T. Ito,
taka.ito@eas.gatech.edu

Citation:
Ito, T., S. Minobe, M. C. Long, and C. Deutsch (2017), Upper ocean O_2 trends: 1958–2015, *Geophys. Res. Lett.*, *44*, 4214–4223, doi:10.1002/2017GL073613.

Received 27 MAR 2017
Accepted 18 APR 2017
Accepted article online 24 APR 2017
Published online 9 MAY 2017

Upper ocean O_2 trends: 1958–2015

Takamitsu Ito[1], Shoshiro Minobe[2,3], Matthew C. Long[4], and Curtis Deutsch[5]

[1]School of Earth and Atmospheric Sciences, Georgia Institute of Technology, Atlanta, Georgia, USA, [2]Department of Natural History Sciences, Graduate School of Science, Hokkaido University, Sapporo, Japan, [3]Department of Earth and Planetary Sciences, Faculty of Science, Hokkaido University, Sapporo, Japan, [4]Climate and Global Dynamics Laboratory, National Center for Atmospheric Research, Boulder, Colorado, USA, [5]School of Oceanography, University of Washington, Seattle, Washington, USA

Abstract Historic observations of dissolved oxygen (O_2) in the ocean are analyzed to quantify multidecadal trends and variability from 1958 to 2015. Additional quality control is applied, and the resultant oxygen anomaly field is used to quantify upper ocean O_2 trends at global and hemispheric scales. A widespread negative O_2 trend is beginning to emerge from the envelope of interannual variability. Ocean reanalysis data are used to evaluate relationships with changes in ocean heat content (OHC) and oxygen solubility ($O_{2,sat}$). Global O_2 decline is evident after the 1980s, accompanied by an increase in global OHC. The global upper ocean O_2 inventory (0–1000 m) changed at the rate of -243 ± 124 T mol O_2 per decade. Further, the O_2 inventory is negatively correlated with the OHC ($r = -0.86$; 0–1000 m) and the regression coefficient of O_2 to OHC is approximately -8.2 ± 0.66 nmol O_2 J^{-1}, on the same order of magnitude as the simulated O_2-heat relationship typically found in ocean climate models. Variability and trends in the observed upper ocean O_2 concentration are dominated by the apparent oxygen utilization component with relatively small contributions from $O_{2,sat}$. This indicates that changing ocean circulation, mixing, and/or biochemical processes, rather than the direct thermally induced solubility effects, are the primary drivers for the observed O_2 changes. The spatial patterns of the multidecadal trend include regions of enhanced ocean deoxygenation including the subpolar North Pacific, eastern boundary upwelling systems, and tropical oxygen minimum zones. Further studies are warranted to understand and attribute the global O_2 trends and their regional expressions.

Plain Language Summary This new paper describes the analysis of the dissolved oxygen in the global ocean using the most recent version of the World Ocean Database for the period of 1955 to 2015. After careful examination of the data, we found that a statistically significant, widespread O_2 decline is emerging beyond the envelope of natural fluctuations. Our study also reveals a tight relationship between O_2 inventories and the ocean heat content. The spatial pattern and magnitude of this relationship are consistent with expectations derived from mechanistic ocean climate models forced under climate warming scenarios. Taken together, the trends we document here are suggestive of the effects of the ocean warming beginning to supersede natural variability and emerge as a recognizable signal. This merits additional scrutiny over the coming years.

1. Introduction

In this and following centuries, marine ecosystems will likely face multiple stressors as a consequence of high CO_2 and a warming climate. The three factors—temperature increase, ocean acidification, and ocean deoxygenation—are global-scale phenomena with significant regional variations, influencing the ecosystem and biogeochemical cycles in ways not yet fully documented [*Gruber*, 2011]. Unraveling the nature and the consequences of these changes is one of the grand challenges for the ocean science community. The three factors are related to one another that deoxygenation likely results in increased ocean acidification in subsurface waters. Such waters commonly supply nutrient to continental shelves, especially in upwelling regions. Thus, a better understanding of deoxygenation will improve our understanding of ocean acidification.

Earth System Model (ESM) simulations predict that the ocean's O_2 content is sensitive to climate warming, suggesting a significant decline of global O_2 inventory under warming scenarios out to 2100 [*Keeling et al.*, 2010]. While widespread O_2 decline in the extratropical thermocline is a robust projection of the current

generation of the ESMs, there are significant differences among models especially in the tropics [*Bopp et al.*, 2013; *Cocco et al.*, 2013]. In a warming climate, increasing seawater temperature decreases oxygen solubility, thereby reducing concentrations assuming all other factors being equal. Furthermore, increased upper ocean stratification associated with surface warming (and increased precipitation and glacier melt) can weaken ventilation, the exchange of well-oxygenated surface waters with the interior ocean. These two mechanisms reinforce one another to deplete the subsurface oxygen on the centennial time scale [*Bopp et al.*, 2002; *Plattner et al.*, 2002].

Numerous attempts have been made to detect low-frequency variability and long-term trends of subsurface O_2 using historic data sets [*Andreev and Baturina*, 2006; *Emerson et al.*, 2004; *Helm et al.*, 2011; *Johnson and Gruber*, 2007; *Ono et al.*, 2001; *Sasano et al.*, 2015; *Stendardo and Gruber*, 2012; *Stramma et al.*, 2008; *van Aken et al.*, 2011; *Whitney et al.*, 2007; *Schmidtko et al.*, 2017]. Analysis of historic data sets poses significant challenges due to sparse and irregular sampling, making the detection of long-term trends a signal-noise problem [*Long et al.*, 2016]. The global compilation by *Garcia et al.* [2005] revealed significant decadal variability of O_2, apparent oxygen utilization (AOU), and heat content in the upper 100 m for the period of 1955 through 1998. In this time period the magnitude of long-term linear trends of O_2 and AOU is relatively small compared to the decadal-scale fluctuations. *Schmidtko et al.* [2017] included additional data through recent years to calculate the O_2 trends, reporting a significant long-term trend at the rate of -257.5 ± 185.1 T mol O_2 (T mol = 10^{12} mol) per decade for the upper 1200 m of global oceans, equivalent of about $2 \pm 1.5\%$ loss of the O_2 inventory for the last 50 years. In this study we build on these previous observational efforts; we examine trends in global-scale upper ocean oxygen for the period 1958 through 2015 and examine its relationship with the ocean heat content (OHC) changes.

2. Method

Additional quality control is applied to develop objectively mapped monthly climatologies of O_2 based on the World Ocean Database 2013 (WOD13) [*Boyer et al.*, 2013] at standard depths specified in the data set. We use an iterative process to construct observationally based O_2 anomaly fields. Initially, we assemble monthly climatologies using all available data. We then construct the O_2 anomaly fields by subtracting the monthly climatologies from the observed O_2 values. Then we perform the quality control to remove questionable data points that are defined as outliers beyond 3 times the standard deviation of the anomalies at each point in space. When the questionable data points are removed, we recalculate the monthly climatologies and repeat the quality control procedure twice in order to minimize questionable data points and biases in climatologies. Anomaly data are binned annually, and the baseline for the anomalies is referenced to the 1950–2015 long-term mean. The resulting O_2 anomaly fields are then objectively mapped onto the global $1° \times 1°$ latitude/longitude grid for each standard depth. A Gaussian weight function is used for the objective mapping with the zonal and meridional length scales of 1000 km and 500 km, respectively. The data coverage is sparse and uneven, and the sampling density is particularly low in remote regions such as the central subtropical gyres. While the relatively large radius of influence is used to reduce data gaps, it can erroneously blend information across physically separated waters, for example, between marginal seas and open oceans. Regional masks are used for the Mediterranean Sea and the Japan Sea, but for the other marginal seas the data from the nearby open ocean can be blended in, which requires caution in the interpretation.

The distribution of O_2 solubility is estimated using temperature and salinity from ocean reanalysis products: the European Centre for Medium-Range Weather Forecasts Ocean Reanalysis (ORAS4) [*Balmaseda et al.*, 2013] and the Simple Ocean Data Assimilation (SODA version 2.2.4) [*Carton et al.*, 2000]. Rather than using raw data, we rely on the data assimilation products that are dynamically consistent and are constrained by a suite of hydrographic and satellite observations. For each product, we sample the temperature and salinity at the time and location of the O_2 data points and calculate corresponding oxygen solubility ($O_{2,sat}$) [*Garcia and Gordon*, 1992]. This calculation allows us to separate O_2 variability into two components: (1) anomalies driven by changes in the solubility of O_2 and (2) anomalies driven by changes in the apparent oxygen utilization ($-\mathrm{AOU} = O_2 - O_{2,sat}$). We compute the AOU component by residual, subtracting changes that can be explained by solubility from the total O_2 anomaly. The AOU component reflects the cumulative effect of biological O_2 consumption and the preformed O_2 value of the source waters; thus, it depends on ocean circulation, mixing, and biochemical processes. Upper ocean heat content is also calculated using the ocean reanalysis products.

Three factors motivate a focus on O_2 variability in the upper ocean. First, the upper ocean O_2 has significant ecological impacts due to proximity to surface ocean habitats. Second, upper ocean processes are strongly affected by atmosphere-ocean interactions; thus, upper ocean O_2 is likely sensitive to climate variability. Third, the upper ocean is relatively well sampled, enabling more robust analysis with less uncertainty. Even so, significant uncertainty still exists due to the sparse and uneven distribution of data coverage both in time and space. The temporal data coverage is relatively poor in the earliest (1950s) and latest (2010s) part of the time series since some of the latest observations have not yet been included in the database. We examine regional data coverage by counting the number of years with observations for each 1° × 1° cells of the objectively mapped field (see supporting information Figure S1).

With this sparse sampling in mind, we compile the time series of the normalized O_2 inventory in the upper ocean above 1000 m depth by performing the following calculation:

$$I_{O_2}(t) = \left(\frac{V_{obs}(t)}{V_{tot}}\right)^{-1} \int O_2'(\mathbf{x}, t)\, dV, \quad (1)$$

where $O_2'(\mathbf{x}, t)$ is the oxygen anomaly, V_{tot} is the total volume of water, and $V_{obs}(t)$ is the volume of grid cells filled with O_2 data. The volume integration is based on the same standard depths as the World Ocean Database.

The integral in equation (1) is performed with missing data being replaced with zeros, but this produces spurious variability reflecting the year-to-year changes in sampling density. In order to correct for this bias, the inventory is normalized by the volumetric sampling ratio, $(V_{obs}(t)/V_{tot})$. This correction effectively amplifies the signal when a relatively small volume is sampled, implicitly assuming that the global mean O_2 is correctly represented by the sample mean.

In order to examine the potential errors associated with this method of calculating the global O_2 inventory with relatively sparse observations, we analyze a "large" ensemble of simulations conducted with the Community Earth System Model-Large Ensemble (CESM-LE) project [*Kay et al.*, 2015]. The CESM-LE included 35 ensemble members with ocean biogeochemistry output. The model is spun-up to the preindustrial conditions referenced to year 1850, and a single ensemble member was integrated from 1850 to 1920. Additional ensemble members are generated at 1920 by making small ($\mathcal{O}(10^{-14})$ K) perturbations in the air temperature field and integrated for 181 years from 1920 to 2100, forced by historical forcing through 2005 and by the Representative Concentration Pathway 8.5 forcing from 2006 to 2100. The quality of the O_2 simulation is discussed by *Long et al.* [2016]; briefly, the model simulates a realistic distribution of O_2 but tends to have concentrations and variability (including trends) that are biased low. Even though the model is not perfect, many realizations of the oxygen variability fields allow to evaluate the potential sampling bias in the context of a single mechanistic model.

We calculate the subsampled O_2 inventories in the CESM-LE according to the observational sampling pattern including the increased footprint of the data through the objective mapping. The subsampled O_2 inventories are then adjusted according to equation (1). We then compare these to the true O_2 inventories for each ensemble member from 1955 to 2015 (Figure S2). About 86% of the members (30 out of 35 ensembles) estimated the magnitude of the linear trend to be within the range of −30% + 8% of the true trend in the CESM-LE simulations. There is a general tendency that the subsampled O_2 inventories underestimate the true global O_2 trend. In 28 out of 35 ensemble members, the linear trend (1958–2015) of subsampled O_2 inventories underestimates the true trend. This indicates that there are regions outside the observational sampling pattern that have stronger trends in O_2 in the CESM-LE simulations. In general, we are encouraged that the existing observations have enough coverage to yield the correct sign of the global trend and the first-order approximation of its magnitude in the context of the CESM-LE.

3. Results

3.1. Global O_2 Inventory

The normalized global O_2 inventory is plotted in Figure 1a for different depth ranges. Overall the O_2 content increases slightly prior to the mid-1980s, followed by a strong decline after the mid-1980s. This pattern is consistent with the earlier study of *Garcia et al.* [2005] who focused on the upper 100 m inventory for the period of 1955–1998. For the period of 1958 to 2015, the linear trend of upper ocean O_2 inventory (0–1000 m) is −243 ± 124 T mol O_2 (T mol = 10^{12} mol) per decade, in agreement with the result of a recent independent

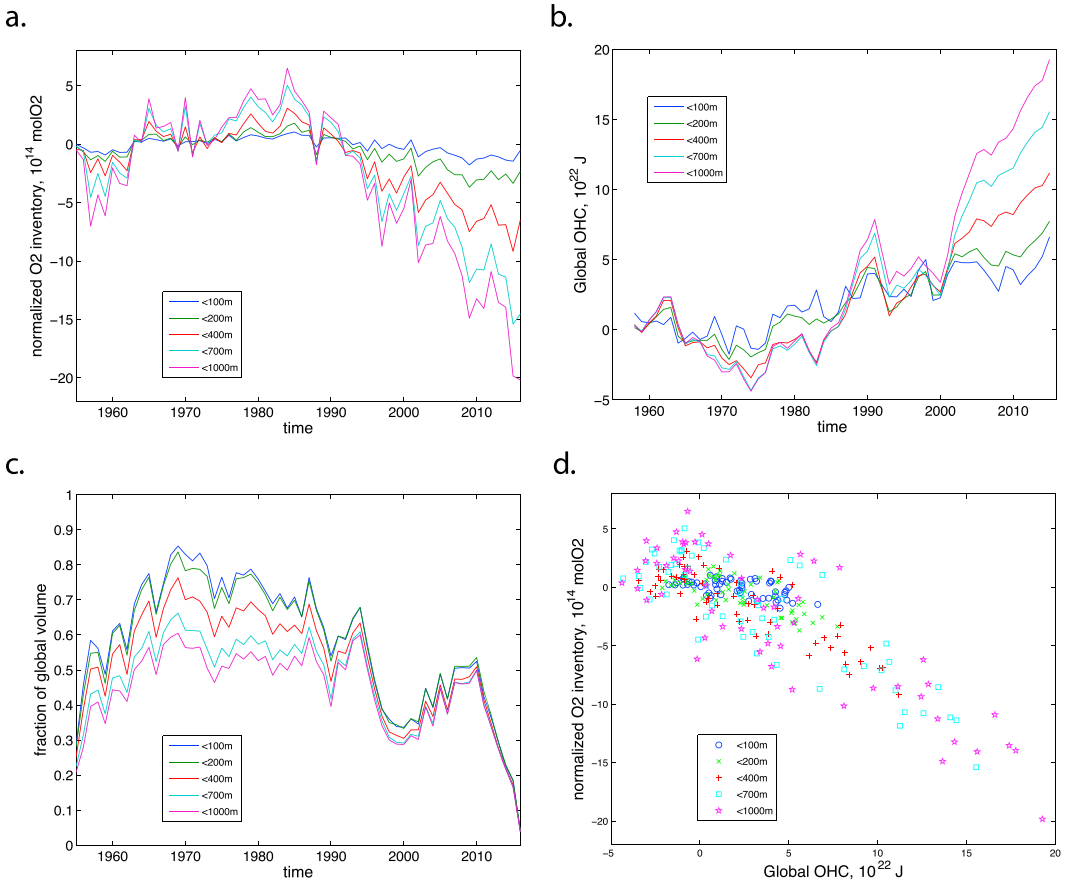

Figure 1. (a) Normalized O_2 inventory above the depths of 100 m (blue), 200 m (green), 400 m (red), 700 m (teal), and 1000 m (purple). (b) Global OHC based on the ORAS4 data set. The color coding is the same as Figure 1a indicating the vertical range of integration. (c) Volumetric sampling density measured as the fraction of grid cells filled with data. (d) The scatter diagram of the normalized O_2 inventory versus OHC. The significance testing of the correlation is performed according to the definition of the effective sample size according to *Bretherton et al.* [1999].

study [*Schmidtko et al.*, 2017]. We find that a similar pattern exists throughout the upper 1000 m of the water column and that the declining trend after the mid-1980s has persisted until recent years. Regression analysis shows that approximately 46% of the variability of the O_2 content occurs above 400 m, and 78% of the variability occurs above 700 m. Figure 1c shows the volumetric sampling ratio, $V_{obs}(t)/V_{tot}$ which is the normalization factor for the O_2 inventory (equation (1)). The sampling ratio generally exceeds 40% between 1960 and 2010, but most recent years have significantly lower sampling ratio, in part because recent data are not yet included in the database. We expect an increased uncertainty for the most recent years due to sparser sampling; the computed O_2 inventory after 2010 may change significantly when all available data are included in the database.

Figure 1b shows the global OHC based on the ORAS4 data set. *Balmaseda et al.* [2013] examine the data sources and their calculation of global OHC in detail. There is a slight difference in the OHC time series between the ORAS4 and the WOD13 which shows a long-term positive trend for the entire time period (see https://www.nodc.noaa.gov/OC5/3M_HEAT_CONTENT/). The time evolution global OHC is dominated by the multidecadal warming trend with a few episodic cooling events. The cooling episodes match with the period of volcanic eruptions (El Chichón in 1982 and Mount Pinatubo in 1991) and the period following the 1997–1998 El Niño event. The normalized O_2 inventory is compared to the OHC time series (Figure 1d). The two time series are significantly correlated according to a t test ($r = -0.86$, 95% confidence interval (CI) for 0–1000 m OHC and O_2).

The regression reveals the relationship between the changes in the OHC and the O_2 inventory. Centennial-scale global warming simulations using ESMs predict that the O_2-heat ratio to be between −5.9 and

−6.7 nmol O_2 J^{-1} [*Keeling et al.*, 2010]. For the normalized O_2 inventory and the OHC above the 1000 m depth, the regression coefficient is −8.2 ± 0.66 nmol O_2 J^{-1}. The overall agreement in the O_2-heat ratio is remarkable given the uncertainties in the inventory calculation and the potential model errors. A close examination of Figure 1d reveals that the slope of O_2-heat relationship is flatter at shallower depths. The O_2-heat ratio is not uniform spatially; the O_2 inventory appears to be less sensitive to the changes in OHC in the shallower waters and the ratio increases with depth (supporting information Table S1). Above the 100 m depth, the regression coefficient is −1.96 ± 1.27 nmol O_2 J^{-1}, consistent with the expected relationship based on the temperature dependence of solubility [*Keeling and Garcia*, 2002]. While the linkages between the O_2 content and OHC are not fully understood, the observation suggests that the O_2 inventory in/below the thermocline is significantly more sensitive to the OHC. This may indicate the crucial role played by the ventilation and the circulation changes of the deeper water masses which may reflect the freshening and warming of the water column. This result is consistent with the recent study by *Schmidtko et al.* [2017] that the O_2 trends above the main thermocline are primarily controlled by the temperature dependence of O_2 solubility and the AOU component becomes dominant in the deeper waters.

3.2. Global and Hemispheric Trends in O_2, $O_{2,sat}$, and AOU

To further investigate the upper ocean O_2 changes, we examine the global and hemispheric area-weighted mean O_2 time series for three depth levels at 100 m, 200 m, and 400 m. We include results from the 200 m depth as Figure 2 in the main text; data from the 100 m and 400 m depths are also shown in the supporting information (Figures S3 and S4). Our calculation of the linear trend and its statistical significance is based on the method of adjusted standard error and adjusted degrees of freedom following *Santer et al.* [2000], wherein a *t* test is used to evaluate whether or not the observed linear trend is significantly different from zero. Figures 2a, 2c, and 2e show the global and hemispheric time series of O_2, O_2^{sat}, and the negative of AOU at the depth of 200 m. As described above, we compute the negative of AOU as a residual, subtracting the solubility component from the total O_2 anomaly; thus, the AOU component captures the O_2 variability not explained by the solubility changes. There are two estimates of O_2^{sat} from the ORAS4 and SODA2.2.4 products which have different temperature/salinity distributions. The two reanalyses agree in the overall magnitude of the $O_{2,sat}$ variability which is much smaller than that of O_2; therefore, regardless of the reanalysis product, the AOU component dominates the O_2 variability and so we plot AOU based on ORAS4 only.

The two hemispheres both exhibit multidecadal O_2 decline, but their temporal variabilities are different. It is important to note that the data density of the Southern Hemisphere is significantly lower than the Northern Hemisphere; thus, it is more likely influenced by the sampling biases. With this caveat in mind, the global and hemispheric O_2 time series show significant decline after the 1980s, which is also evident at 100 m and 400 m depths (see Figures S3 and S4). At 100 m depth, there is a decadal O_2 increase from the 1960s to 1980s for the global and northern hemispheric data as previously identified [*Garcia et al.*, 2005]. Previous investigations of regional O_2 changes have also shown strong O_2 decline in the Pacific basin after the 1980s [*Deutsch et al.*, 2011; *Czeschel et al.*, 2012; *Stramma et al.*, 2012; *Ito and Deutsch*, 2013], which may be related to the reduced ventilation in the Sea of Okhotsk [*Ohshima et al.*, 2014; *Nakanowatari et al.*, 2007].

Figures 2b, 2d, and 2f show the global and hemispheric linear trends of O_2 represented as a matrix of trends with varying starting and ending years. The color shading indicates the magnitude of the linear trend and the hatched regions indicate whether the trend is significantly differ from zero (positive or negative) with 95% confidence interval [*Santer et al.*, 2000]. The linear trends are sensitive to the time period of analysis due to the superposition of interannual variability with the multidecadal trends. Overall, the trend matrix is predominantly negative, and the decreasing trends become statistically significant with the ending year of 2005 and later. The earlier analysis [*Garcia et al.*, 2005] indeed detected the beginning of post-1980s O_2 decline, despite the relatively narrow time window (1955–1998). Our analysis shows that the negative trend continued to develop during 2000s.

3.3. Spatial Pattern of the O_2 Trend

Figure 3 shows the maps of the multidecadal trend over three different depth ranges. There are several regions of intense O_2 decline as noted by earlier investigations such as western subpolar North Pacific [*Ono et al.*, 2001], the Gulf of Alaska [*Whitney et al.*, 2007], equatorial Atlantic, and eastern equatorial Pacific [*Stramma et al.*, 2008, 2012]. The subpolar North Pacific (SPNP) is a relatively well sampled region and exhibits a significant negative trend at all depths as shown by earlier studies [*Ono et al.*, 2001; *Whitney et al.*, 2007]. There are also several

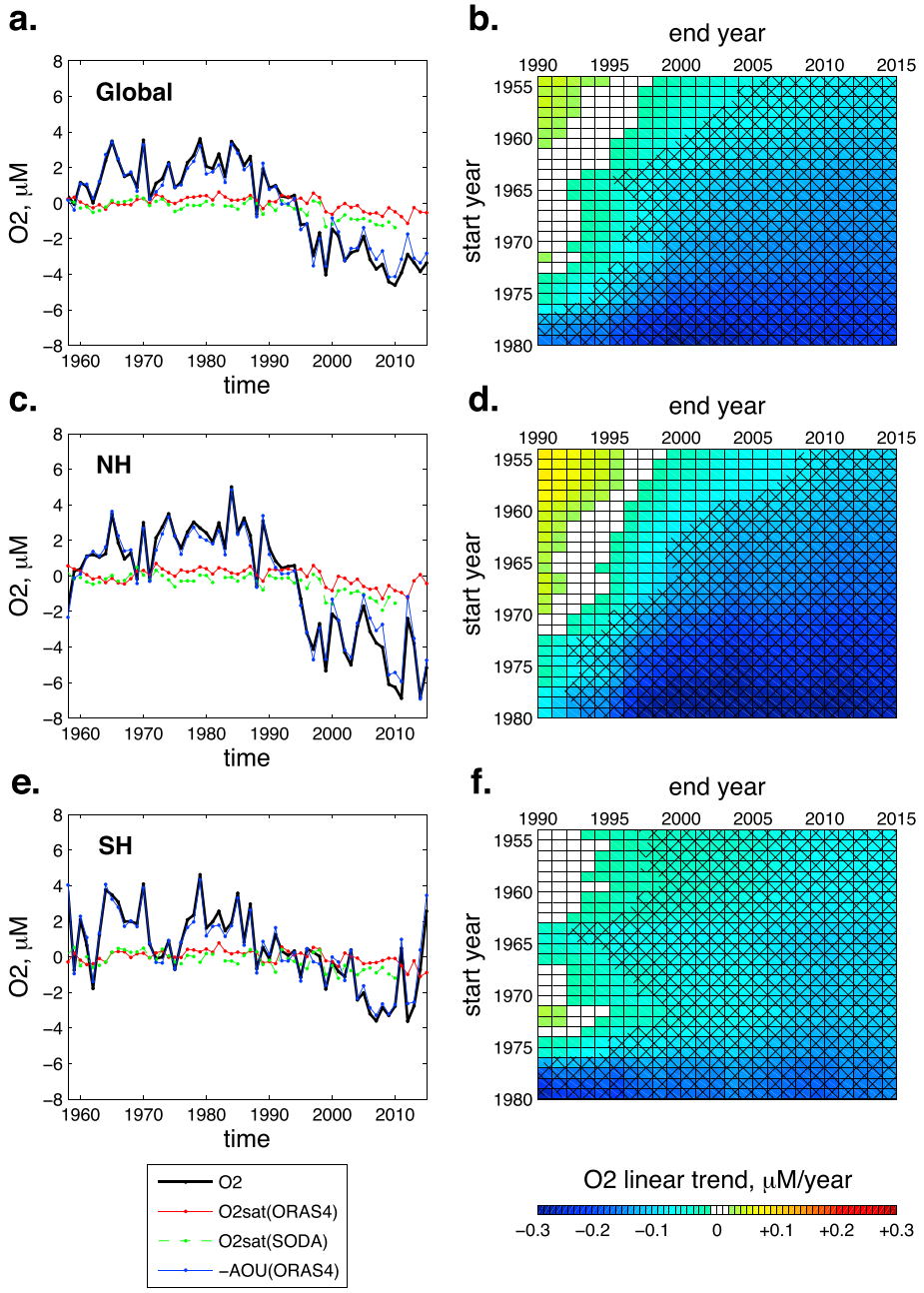

Figure 2. (a) Global O_2 time series at the depth of 200 m. Data points are weighted by the cosine of latitude. Black is O_2; red and green are O_2 saturation based on ORAS4 and SODA2.2.4 respectively. Blue is (−1) × AOU. (b) Trend matrix is formed by taking linear trend of O_2 with different starting and ending years. Color shading shows the magnitude of the trend. Hatching is applied for positive/negative definite trends with 95% CI using the method of adjusted standard error and adjusted degree of freedom following *Santer et al.* [2000]. (c, d) The same as Figures 2a and 2b but for the northern hemispheric data points only. (e, f) The same as Figures 2a and 2b but for the southern hemispheric data points only.

regions of O_2 increase such as in the western subtropical North Pacific and eastern subpolar North Atlantic as noticed by previous studies [*Helm et al.*, 2011; *Sasano et al.*, 2015].

Many parts of the global oceans are undersampled, and the apparent lack of trend may be an artifact of sparse observations in some regions. The open oceans in the extratropical Southern Hemisphere are poorly sampled in general (Figure S1), and it is possible that the relatively weak trend in the Southern Hemisphere (Figure 3) may be due to the sparse sampling. In contrast, the Labrador Sea is a relatively well sampled region, but the observations do not show a significant trend there. Convective mixing and hydrographic properties of the

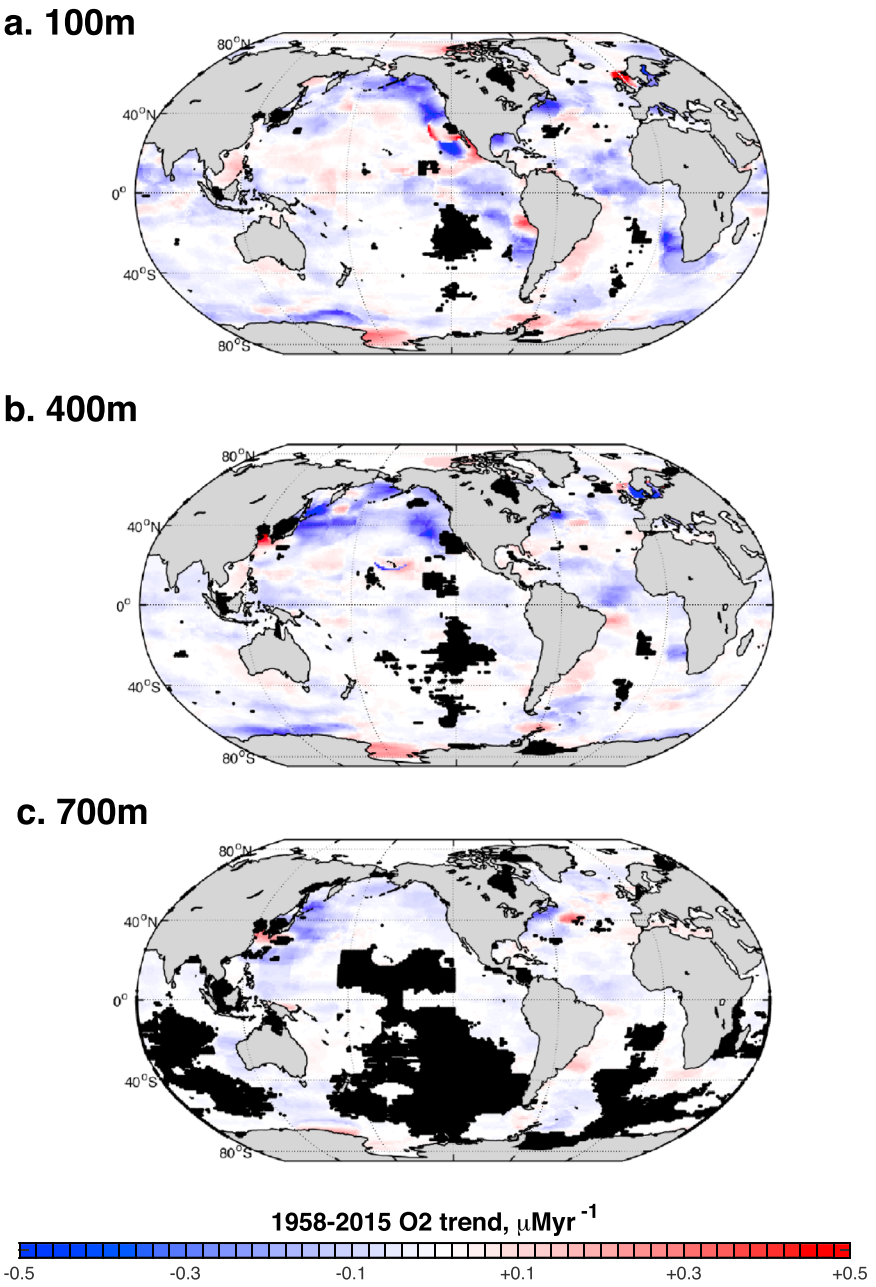

Figure 3. (a) Global map of the linear trend of O_2 time series at the depth of 100 m. We plot the linear trend for the grid cells where the effective sample size (N_{eff}) is greater than 20. (b) Same as Figure 3a but at the depth of 400 m. (c) Same as Figure 3a but at the depth of 700 m. We indicate the regions where there are insufficient data ($N_{eff} < 20$) by black dots.

Labrador Sea are known to exhibit significant interannual and decadal variability, but no significant long-term trend has been observed to date [*Yashayaev*, 2007; *van Aken et al.*, 2011]. Thus, a long-term trend of O_2 is not expected in this region, and our result is consistent with these earlier studies.

Finally, we attempt to speculate the potential causes of the observed O_2 changes. Solubility changes only play a secondary role below the thermocline, given the relatively low variability in the $O_{2,sat}$ component; thus, the O_2 variability is predominantly controlled by AOU changes for the global averages. The changes in AOU can come from many factors: the preformed O_2 value at the location of water mass formation, the rates of biochemical O_2 consumption, the rates of subduction, eddy mixing, and shifts in water mass boundaries. The circulation and eddy stirring can modulate the physical supply of O_2 affecting the regional patterns of O_2 changes [*Stramma et al.*, 2010; *Czeschel et al.*, 2011; *Llanillo et al.*, 2013; *Brandt et al.*, 2015]. Figure 3 shows

the contrast between the subpolar and subtropical North Pacific where the O_2 strongly decreases in the subpolar region and it slightly increases in the subtropics. The increase of subtropical O_2 is consistent with the expansion of winter time isopycnal outcrop where O_2-rich surface waters subduct into the thermocline [*Kwon et al.*, 2016]. In the subpolar region the thermocline waters are not directly ventilated from the open ocean but the source waters are formed in the marginal seas of the northwestern North Pacific and are strongly influenced by the mixing at the Oyashio front and Kuroshio extension regions [*Talley*, 1993]. The O_2 decline in the SPNP may reflect the changes in the source regions such as the Sea of Okhotsk or the mixing processes. In the tropical oxygen minimum zones, the ocean climate and circulation variability can shift water masses and alter the rate of nutrient supply to the surface euphotic layer and drive decadal O_2 variability [*Deutsch et al.*, 2011].

4. Discussion

The World Ocean Database 2013 [*Boyer et al.*, 2013] is used to calculate the global O_2 inventory and hemispheric O_2 trends for the period of 1958 to 2015. The distribution of observations is relatively sparse, omitting large regions of the oceans; however, we demonstrate that this distribution is sufficient to robustly estimate global O_2 trends in the context of an Earth System Model simulation. An earlier study [*Garcia et al.*, 2005] with a shorter record period (1955–1998) found little evidence of a long-term trend, but our analysis shows that the addition of 17 years of observations has revealed a widespread negative O_2 trend beginning to emerge from the envelope of interannual variability. In conjunction with the O_2 trend, the O_2 solubility and the ocean heat content is examined using temperature and salinity data from ORAS4 [*Balmaseda et al.*, 2013] and SODA2.2.4 [*Carton et al.*, 2000]. Consistent with previous studies, observed O_2 variability is dominated by AOU changes regardless of the data set used for the temperature and salinity. This indicates that O_2 changes are predominantly driven by changing ocean ventilation and/or biological O_2 consumption. Furthermore, the O_2 inventory is significantly correlated with changes in ocean heat content, particularly for thermocline and deep waters, indicating linkages between the ocean heat uptake and the global AOU increase.

The mechanisms behind the AOU change are not fully understood. In a warming ocean, the surface heating, glacier melt, and increased precipitation at high latitudes can increase the ocean stratification, leading to the weakened mixing of O_2-rich surface waters into the thermocline. Earth System Models indeed predict a long-term O_2 decline (and increase of AOU as well as ventilation age) on the centennial time scales [*Cocco et al.*, 2013; *Bopp et al.*, 2013; *Long et al.*, 2016]. This mechanism could be at play for the last several decades of O_2 data analyzed here.

The observed O_2 decline is not uniform in space. Relatively strong and widespread O_2 decline is found in the subpolar North Pacific and in the tropics, whereas the subtropical North Pacific shows a moderate O_2 increase. This pattern has been identified by earlier studies in association with increasing upper ocean stratification [e.g., *Ono et al.*, 2001; *Emerson et al.*, 2004; *Stramma et al.*, 2012], and *Ito et al.* [2016] showed that this pattern may have been caused by the combined effects of natural climate variability and the deposition of polluted dust over the North Pacific Ocean. A recent study [*Long et al.*, 2016] showed that the spatial patterns of O_2 change are similar between the centennial, anthropogenically forced trend and interannual variability. On this basis, it is possible that the strong O_2 change in the subpolar North Pacific can be caused by natural climate variability, warming-induced long-term change, or some combination of the two.

While climate trends and variability are clearly important drivers of observed O_2 changes, a wider range of processes can contribute to the O_2 changes. For example, *Riebesell et al.* [2007] showed that the C:N utilization ratio of organic matter production in a mesocosm experiment increased under high-CO_2 conditions. If this relationship scales globally, the effect could yield larger C:N ratios in sinking organic matter, thereby driving subsurface oxygen declines under high-CO_2 conditions (presuming C:O_2 stoichiometry of aerobic respiration remains the same). This effect was included in a modeling study [*Oschlies et al.*, 2008], which showed a 50% increase in the global volume of suboxic ($O_2 < 5\mu M$) waters by 2100 due to increasing C:N ratios in sinking organic matter relative to experiments omitting this effect. In addition to changing C:N utilization ratios, increased exogenous nutrient inputs could drive increased carbon export and oxygen utilization in the interior. *Krishnamurthy et al.* [2010], for instance, simulated anthropogenic enhancements of aerosol nutrient deposition in an Earth System Model. Their simulation showed an increase in the biological productivity in the Pacific basin stimulated by the additional nutrient input from aerosols. Interestingly, the simulated O_2 change in the North Pacific was only moderate in this particular model, and the authors commented that the circulation variability may be more important in driving O_2 variability in this region.

While these perturbations to nutrient cycling could alter the O_2 trends over time, our result reveals a tight relationship between O_2 inventories and OHC. The spatial structure and magnitude of this relationship are consistent with expectations derived from mechanistic models forced under climate warming scenarios. This study owes its existence to the international collaboration through the World Ocean Database Project, and it is crucial to maintain and support the collection and submission of the data. Unfortunately, the spatiotemporal distribution of O_2 observations remains too sparse for definitive conclusions and attribution. However, taken together, the evidence is consistent with anthropogenic warming acting as the primary driver of long-term trends in ocean O_2. The trends we document are suggestive of the effects of warming beginning to supersede natural variability and emerge as a recognizable signal. This merits additional scrutiny over the coming years; if it is the warming signal, we should expect to see continued widespread declines in oceanic O_2. The impacts of ocean deoxygenation on ocean ecosystems may be profound. In this light, it is critical to develop improved understanding of the mechanisms driving trends and variability in the oceanic O_2. The scientific community should work to ensure that adequate observing capabilities are maintained; we have an obligation to document and communicate these impacts of warming, such that society can make informed decisions and understand costs/benefits trade-offs for mitigation.

Acknowledgments
We are thankful for the support from the Scientific Visitor Program of the Climate and Global Dynamics Laboratory at the National Center for Atmospheric Research (NCAR) as this study started, while the authors were visiting NCAR during the summer of 2016. NCAR is supported by the National Science Foundation. T.I. is partially supported by the NSF (OCE-1357373) and NOAA grant (NA16OAR4310173). S.M. is supported by the Japan Society for the Promotion of Science (JSPS) KAKENHI (26287110, 26610146, and 15H01606). All data sets supporting the conclusions of this study are available in the public domain as referenced within the paper. Data analysis products used to generate the figures and tables are available from the corresponding author upon request.

References

Andreev, A. G., and V. I. Baturina (2006), Impacts of tides and atmospheric forcing variability on dissolved oxygen in the subarctic North Pacific, *J. Geophys. Res.*, *111*, C07S10, doi:10.1029/2005JC003103.

Balmaseda, M. A., K. Mogensen, and A. T. Weaver (2013), Evaluation of the ECMWF ocean reanalysis system ORAS4, *Q. J. R. Meteorol. Soc.*, *139*(674), 1132–1161, doi:10.1002/qj.2063.

Bopp, L., C. Le Quéré, M. Heimann, A. C. Manning, and P. Monfray (2002), Climate-induced oceanic oxygen fluxes: Implications for the contemporary carbon budget, *Global Biogeochem. Cycles*, *16*, 1022, doi:10.1029/2001GB001445.

Bopp, L., et al. (2013), *Biogeosciences*, *10*, 6225–6245, doi:10.5194/bg-10-6225-2013.

Boyer, T., et al. (2013), World Ocean Database 2013, in *NOAA Atlas NESDIS*, vol. 72, edited by S. Levitus and A. Mishonov, 209 pp., Silver Springs, Md., doi:10.7289/V5NZ85MT.

Brandt, P., et al. (2015), On the role of circulation and mixing in the ventilation of oxygen minimum zones with a focus on the eastern tropical North Atlantic, *Biogeosciences*, *12*(2), 489–512, doi:10.5194/bg-12-489-2015.

Bretherton, C. S., M. Widmann, V. P. Dymnikov, J. M. Wallace, and I. Bladé (1999), The effective number of spatial degrees of freedom of a time-varying field, *J. Clim.*, *12*(7), 1990–2009, doi:10.1175/1520-0442(1999)012<1990:TENOSD>2.0.CO;2.

Carton, J. A., G. Chepurin, X. Cao, and B. Giese (2000), A simple ocean data assimilation analysis of the global upper ocean 1950–95. Part I: Methodology, *J. Phys. Oceanogr.*, *30*(2), 294–309, doi:10.1175/1520-0485(2000)030<0294:ASODAA>2.0.CO;2.

Cocco, V., et al. (2013), Oxygen and indicators of stress for marine life in multi-model global warming projections, *Biogeosciences*, *10*, 1849–1868, doi:10.5194/bg-10-1849-2013.

Czeschel, R., L. Stramma, F. U. Schwarzkopf, B. S. Giese, A. Funk, and J. Karstensen (2011), Middepth circulation of the eastern tropical South Pacific and its link to the oxygen minimum zone, *J. Geophys. Res.*, *116*, C01015, doi:10.1029/2010JC006565.

Czeschel, R., L. Stramma, and G. C. Johnson (2012), Oxygen decreases and variability in the eastern equatorial Pacific, *J. Geophys. Res.*, *117*, C11019, doi:10.1029/2012JC008043.

Deutsch, C., H. Brix, T. Ito, H. Frenzel, and L. Thompson (2011), Climate-forced variability of ocean hypoxia, *Science*, *333*(6040), 336–339, doi:10.1126/science.1202422.

Emerson, S., Y. Watanabe, T. Ono, and S. Mecking (2004), Temporal trends in apparent oxygen utilization in the upper pycnocline of the North Pacific: 1980–2000, *J. Oceanogr.*, *60*(1), 139–147, doi:10.1023/B:JOCE.0000038323.62130.a0.

Garcia, H. E., and L. I. Gordon (1992), Oxygen solubility in seawater: Better fitting equations, *Limnol. Oceanogr.*, *37*(6), 1307–1312, doi:10.4319/lo.1992.37.6.1307.

Garcia, H. E., T. P. Boyer, S. Levitus, R. A. Locarnini, and J. Antonov (2005), On the variability of dissolved oxygen and apparent oxygen utilization content for the upper world ocean: 1955 to 1998, *Geophy. Res. Lett.*, *32*, L09604, doi:10.1029/2004GL022286.

Gruber, N. (2011), Warming up, turning sour, losing breath: Ocean biogeochemistry under global change, *Philos. Trans. R. Soc.*, *369*, 1980–1996, doi:10.1098/rsta.2011.0003.

Helm, K. P., N. L. Bindoff, and J. A. Church (2011), Observed decreases in oxygen content of the global ocean, *Geophy. Res. Lett.*, *38*, L23602, doi:10.1029/2011GL049513.

Ito, T., and C. Deutsch (2013), Variability of the oxygen minimum zone in the tropical North Pacific during the late twentieth century, *Global Biogeochem. Cycles*, *27*(4), 1119–1128, doi:10.1002/2013GB004567.

Ito, T., A. Nenes, M. S. Johnson, N. Meskhidze, and C. Deutsch (2016), Acceleration of oxygen decline in the tropical Pacific over the past decades by aerosol pollutants, *Nat. Geosci.*, *9*(6), 443–447, doi:10.1038/ngeo2717.

Johnson, G. C., and N. Gruber (2007), Decadal water mass variations along 20°W in the northeastern Atlantic Ocean, *Prog. Oceanogr.*, *73*, 277–295, doi:10.1016/j.pocean.2006.03.022.

Kay, J. E., et al. (2015), The Community Earth System Model (CESM) large ensemble project a community resource for studying climate change in the presence of internal climate variability, *Bull. Am. Meteorol. Soc.*, *96*(8), 1333–1349, doi:10.1175/bams-d-13-00255.1.

Keeling, R. F., and H. E. Garcia (2002), The change in oceanic O_2 inventory associated with recent global warming, *Proc. Natl. Acad. Sci. U.S.A.*, *99*(12), 7848–7853, doi:10.1073/pnas.122154899.

Keeling, R. F., A. Körtzinger, and N. Gruber (2010), Ocean deoxygenation in a warming world, *Ann. Rev. of Mar. Sci.*, *2*, 199–229, doi:10.1146/annurev.marine.010908.163855.

Krishnamurthy, A., J. K. Moore, N. Mahowald, C. Luo, and C. S. Zender (2010), Impacts of atmospheric nutrient inputs on marine biogeochemistry, *J. Geophys. Res.*, *115*, G01006, doi:10.1029/2009JG001115.

Kwon, E. Y., C. Deutsch, S.-P. Xie, S. Schmidtko, and Y.-K. Cho (2016), The North Pacific oxygen uptake rates over the past half century, *J. Clim.*, *29*(1), 61–76, doi:10.1175/JCLI-D-14-00157.1.

Llanillo, P. J., J. Karstensen, J. L. Pelegrí, and L. Stramma (2013), Physical and biogeochemical forcing of oxygen and nitrate changes during El Niño/El Viejo and La Niña/La Vieja upper-ocean phases in the tropical eastern South Pacific along 86°W, *Biogeosciences*, *10*(10), 6339–6355, doi:10.5194/bg-10-6339-2013.

Long, M. C., C. A. Deutsch, and T. Ito (2016), Finding forced trends in oceanic oxygen, *Global Biogeochem. Cycles*, *30*, doi:10.1002/2015GB005310.

Nakanowatari, T., K. I. Ohshima, and M. Wakatsuchi (2007), Warming and oxygen decrease of intermediate water in the northwestern North Pacific, originating from the sea of okhotsk, 1955–2004, *Geophys. Res. Lett.*, *34*, L04602, doi:10.1029/2006GL028243.

Ohshima, K. I., T. Nakanowatari, S. Riser, Y. Volkov, and M. Wakatsuchi (2014), Freshening and dense shelf water reduction in the Okhotsk Sea linked with sea ice decline, *Prog. Oceanogr.*, *126*, 71–79, doi:10.1016/j.pocean.2014.04.020. biogeochemical and physical processes in the Sea of Okhotsk and the linkages to the Pacific Ocean.

Ono, T., T. Midorikawa, Y. W. Watanabe, K. Tadokoro, and T. Saino (2001), Temporal increases of phosphate and apparent oxygen utilization in the subsurface waters of western subarctic Pacific from 1968 to 1998, *Geophy. Res. Lett.*, *28*(17), 3285–3288, doi:10.1029/2001GL012948.

Oschlies, A., K. G. Schulz, U. Riebesell, and A. Schmittner (2008), Simulated 21st century's increase in oceanic suboxia by CO_2-enhanced biotic carbon export, *Global Biogeochem. Cycles*, *22*, GB4008, doi:10.1029/2007GB003147.

Plattner, G.-K., F. Joos, and T. F. Stocker (2002), Revision of the global carbon budget due to changing air-sea oxygen fluxes, *Global Biogeochem. Cycles*, *16*, 1096, doi:10.1029/2001GB001746.

Riebesell, U., et al. (2007), Enhanced biological carbon consumption in a high CO_2 ocean, *Nature*, *450*(7169), 545–U10, doi:10.1038/nature06267.

Santer, B. D., T. M. L. Wigley, J. S. Boyle, D. J. Gaffen, J. J. Hnilo, D. Nychka, D. E. Parker, and K. E. Taylor (2000), Statistical significance of trends and trend differences in layer-average atmospheric temperature time series, *J. Geophys. Res.*, *105*(D6), 7337–7356, doi:10.1029/1999JD901105.

Sasano, D., Y. Takatani, N. Kosugi, T. Nakano, T. Midorikawa, and M. Ishii (2015), Multidecadal trends of oxygen and their controlling factors in the western North Pacific, *Global Biogeochem. Cycles*, *29*, 935–956, doi:10.1002/2014GB005065.

Schmidtko, S., L. Stramma, and M. Visbeck (2017), Decline in global oceanic oxygen content during the past five decades, *Nature*, *542*(7641), 335–339, doi:10.1038/nature21399.

Stendardo, I., and N. Gruber (2012), Oxygen trends over five decades in the North Atlantic, *J. Geophys. Res.*, *117*, C11004, doi:10.1029/2012JC007909.

Stramma, L., G. C. Johnson, J. Sprintall, and V. Mohrholz (2008), Expanding oxygen-minimum zones in the tropical oceans, *Science*, *320*, 655–658, doi:10.1126/science.1153847.

Stramma, L., G. C. Johnson, E. Firing, and S. Schmidtko (2010), Eastern Pacific oxygen minimum zones: Supply paths and multidecadal changes, *J. Geophys. Res.*, *115*, C09011, doi:10.1029/2009JC005976.

Stramma, L., A. Oschlies, and S. Schmidtko (2012), Mismatch between observed and modeled trends in dissolved upper-ocean oxygen over the last 50 yr, *Biogeosciences*, *9*(10), 4045–4057, doi:10.5194/bg-9-4045-2012.

Talley, L. D. (1993), Distribution and formation of North Pacific intermediate water, *J. Phys. Oceanogr.*, *23*(3), 517–537, doi:10.1175/1520-0485(1993)023<0517:DAFONP>2.0.CO;2.

van Aken, H. M., M. Femke de Jong, and I. Yashayaev (2011), Decadal and multi-decadal variability of Labrador Sea Water in the north-western North Atlantic Ocean derived from tracer distributions: Heat budget, ventilation, and advection, *Deep Sea Res., Part I*, *58*, 505–523, doi:10.1016/j.dsr.2011.02.008.

Whitney, F. A., H. J. Freeland, and M. Robert (2007), Persistently declining oxygen levels in the interior waters of the eastern subarctic Pacific, *Prog. Oceanogr.*, *75*, 179–199, doi:10.1016/j.pocean.2007.08.007.

Yashayaev, I. (2007), Hydrographic changes in the Labrador Sea, 1960–2005 (vol 73, pg242, 2007), *Prog. Oceanogr.*, *75*(4), 857–859, doi:10.1016/j.pocean.2007.09.001.